A Foreground Mismatch and Memory Harmonic Distortion Calibration Algorithm for TIADC

Haoyang Shen, *Graduate Student Member, IEEE*, Adam Blaq, *Graduate Student Member, IEEE*, Deepu John, *Senior Member, IEEE*, and Barry Cardiff, *Senior Member, IEEE*

***Abstract*— This paper proposes a foreground digital calibration algorithm that estimates and corrects the offset, gain, and time-skew mismatches for time-interleaved analog-to-digital converters (TIADCs) furthermore our algorithm is designed to correct for harmonic distortion introduced by the presence of a nonlinear front-end. We propose a novel simplified non-linear model in place of the more complex conventional Volterra series based structure. The mismatch estimation technique based on the Fast Fourier Transform (FFT) is proposed to estimate the various time-interleaving mismatches simultaneously. A Taylor-based technique is applied to compensate for these mismatches. We also consider the choice of an appropriate time reference for the time-skew correction algorithm by theoretical analysis. The nonlinear distortion correction technique is based on estimating and inverting an assumed 3rd order nonlinearity with a fractional delay. To do this, we design a customized filter in an offline process. Our algorithms are designed to operate in any Nyquist zone. The proposed techniques are verified by a Xilinx Zynq UltraScale+ RFSoC ZCU111 evaluation kit containing a 12-bit, 4.096 GHz TI-ADC with 8 sub-ADCs operating in the 2nd Nyquist zone. Accordingly, we observed an improvement in SFDR of 14 dB for mismatch calibration alone and up to another 12 dB with nonlinear correction enabled.**

***Index Terms*— Time-interleaved analog-to-digital converter (TIADC), fast Fourier transform (FFT), nonlinearity, foreground calibration.**

I. Introduction

TIME-INTERLEAVED analog-to-digital Converter (TIADC) is essential for a wide range of technologies due to its high conversion rates; however, this architecture is sensitive to the offset, gain and time-skew mismatches [1], [2], [3]. These mismatches degrade the performance of a TIADC system. As progress in digital circuits has dramatically outpaced the performance growth of analog circuits, It is common to use digital calibration to compensate the time-interleaved mismatch [4], [5], [6], [7], [8], [9], [10], [11], [12], [13], [14], [15], [16], [17], [18], [19], [20], [21], [22], [23], [24]. Associated with all ADCs is an analog front end (AFE) which we usually model as an amplifier circuit positioned before the ADC core itself [25]. To satisfy the requirements of modern ADC systems, it is important that this AFE be highly linear, which in turn results in a large circuit area and/or energy consumption [26]. One approach is to use an open-loop amplifier, as per [25] and [26], which is low power, low noise, and high bandwidth, but it suffers from nonlinear behavior, ultimately limiting the performance of the entire ADC system; thus, a digital inverse calibration is applied in an attempt to negate the nonlinear distortion [26], [27], [28], [29]. The memoryless nonlinear correction may only be used for the narrowband signals [30], and for the wideband signals and most signals, the nonlinear memory effects must be considered in the digital correction algorithms [31]. Most nonlinear system structures are based on the Volterra series [32], which is complicated to design and needs a large hardware cost and power consumption.

The mismatch and harmonic calibrations are either foreground or background, depending on the estimation technique. The foreground calibration in [4], [5], [6], [8], and [7] uses a training signal that we know its prior knowledge, which we can obtain a more accurate mismatch estimation and faster convergence than the background calibration. However, it cannot track the changes due to process, voltage, and temperature (PVT). In the background calibration in [10], [11], [12], [13], [15], and [14], we know less prior knowledge of input signal. The mismatch can be tracked by taking advantage of some assumed statistical signal properties. It can be operated at a normal process but is less accurate than the foreground calibration. Note that it may not be suitable for all types of signals due to the algorithm constraints.

Some published TIADC background mismatch calibration algorithms [10], [11], [12], [13], [14] can be confused by the presence of various 'pathological' inputs signals, which may cause them not to meet some required system performance (as discussed in Section III-D below). In this work, being a foreground calibration algorithm, we have the freedom to choose the input frequencies such that any additional terms (e.g. HD2 and HD3) occurring as a results of the non-linear front-end do not overlap (in the frequency domain) with any components arising from the TIADC mismatches. This enables us, by means of frequency domain processing, to uniquely separate the effects of non-linear and mismatch calibrations. This compare to many time domain mismatch calibrations e.g. [4], [9]. As with all frequency domain approaches [21],

Manuscript received 31 August 2022; revised 18 November 2022 and 8 December 2022; accepted 11 December 2022. Date of publication 19 December 2022; date of current version 27 February 2023. This work was supported by the China Scholarship Council. This article was recommended by Associate Editor A. Worapishet. *(Corresponding author: Haoyang Shen.)*

The authors are with the School of Electrical and Electronic Engineering, University College Dublin, Dublin 4, D04 V1W8 Ireland (e-mail: haoyang.shen@ucdconnect.ie; adam.blaq@ucdconnect.ie; deepu.john@ucd.ie; barry.cardiff@ucd.ie).

Color versions of one or more figures in this article are available at https://doi.org/10.1109/TCSI.2022.3229208.

Digital Object Identifier 10.1109/TCSI.2022.3229208

[22], [23] we can take advantage of the FFT algorithm to compute the various signal components efficiently. Depending on the number of samples used FFT based approaches can be computationally comparable or less than some time-domain approaches, for example, the LMS algorithm [10], [15] and the genetic algorithm [7].

For the previous FFT-based references, the authors in [21] only estimate the offset and gain mismatch and ignore the time-skew mismatch. The presence of gain and time-skew mismatch affects each other's estimation; thus, it is essential to jointly estimate the gain and time-skew mismatches. The calibration algorithm in [23] and [22] have to use extra steps to estimate the offset mismatch and must use one specific sub-ADC as the reference. The various options of time reference are introduced in [15], [16], [17], and [18], e.g., using zero, sub-ADC, the mid-range point, and extra reference ADC as a time reference. The selection of time reference will affect the dynamic correction range and furthermore the performance of time-skew correction algorithms.

In this work, we propose a foreground calibration algorithm that can jointly estimate and correct the mismatches and additionally consider the impact of nonlinear AFEs. These two issues have separately been considered in the literature previously [7], [8], [10], [29], [33]. However, in this work, we consider the interaction between these two non-ideal aspects of the ADC, for example, the AFE will generate harmonics that can serve to confuse the estimation of the TIADC mismatch parameters which in turn will impact the performance of the AFE correction algorithm. For this reason, we present both the mismatch and non-linear correction algorithms jointly and take steps to ensure mutual compatibility. Except for the mismatch tones, the most prominent SFDR-limiting spur is the third-order harmonic (HD3) [27]. Thus, we propose a simplified memory nonlinear model to replace the conventional Volterra series structure to reduce the design complexity.

Compared with previous FFT-based calibration algorithms, our algorithm can simultaneously estimate offset, gain, and time-skew mismatches, applied for any M-channel (M $\geq$ 2) TIADCs, with no restrictions on reference selection, cannot be affected by nonlinear distortion and has a strong tolerance for background noise. According to previous combined mismatches analysis, the frequency locations of the tones caused by mismatches are fixed and known [1]; thus, the multi-tone ground truth estimation [34] is used to measure the amplitude and phase (complex value) of these tones. These mismatches are estimated by using the inverse of the FFT operation as per Section III. For the mismatch correction, we use the Taylor-based technique to compensate for the time-skew mismatch. The conventional differentiator filter design in [35] only works in the first Nyquist zone. The authors in [20] propose a differentiator design with the help of a Hilbert transform filter that we can compute the derivative of the input at about 90% (0.05–0.95) within any Nyquist zones. We present the theoretical statistic analysis to illustrate that an appropriate time reference significantly reduces the dynamic correction range and further influences the performance of time-skew correction.

When the mismatch calibration is done, we use the multi-tone ground truth estimation algorithm to estimate the amplitude and phase of the fundamental and HD3 for the input signals sweeping the frequency across the full band of operation. Then we can design a customized FIR filter with desired amplitude and phase response in the offline training process and invert an assumed 3rd nonlinearity with a fixed filter in the run-time process.

This paper is organized as follows: the TIADC model with AFE is introduced in Section II. In Section III, we propose an FFT-based estimation algorithm that estimates the offset, gain, and time-skew mismatches and correction structure. Section IV introduces nonlinearity algorithm to recover the harmonic distortion. The statistic analysis of reference selection is presented in Section V. The results are shown in Section VI. Finally, conclusions are drawn in Section VII.

II. TIADC Model With Non-Linear Front-End

A. TIADC With Linear Front End and Sinusoidal Input

In general, an M-channel TIADC system suffers from the offset, gain and time-skew mismatches. In this part, we ignore the nonlinearity and consider the input to be a sinusoidal signal that can be defined as:

$$x(t) \triangleq \beta sin(\omega_{in} t + \theta) \tag{1}$$

where β is the input amplitude, θ is the input phase, and $\omega_{in} \in [0, \pi]$ is defined as the normalised angular frequency.

Let o_m, g_m and τ_m denote the offset, gain and time-skew mismatches of m^{th} sub-ADC, where we assume that $\sum_m o_m = \sum_m g_m = \sum_m \tau_m = 0$ are derived in Appendix A. Hence the TIADC output, $y[n]$, can be expressed as:

$$y[n] = (1 + g[n])\mathcal{A} sin(\omega_{in}(n + \tau[n]) + \phi) + o[n] \tag{2}$$

where $\mathcal{A}$ is defined as the TIADC output amplitude and ϕ is defined as the TIADC output phase. $o[n] \triangleq o_{n(\text{mod } M)}$, $g[n] \triangleq g_{n(\text{mod } M)}$ and $\tau[n] \triangleq \tau_{n(\text{mod } M)}$ respectively. M defined as the number of sub-ADC.

Using the small angle approximation[1] we can rewrite (2) as:

$$\begin{aligned} y[n] &\simeq (1 + g[n])\mathcal{A}\{sin(\omega_{in} n + \phi) + \tau[n]\omega_{in} cos(\omega_{in} n + \phi)\} \\ &\quad + o[n] \\ &= x[n] + e_g[n] + e_\tau[n] + \mathcal{A}\omega_{in} g[n]\tau[n] cos(\omega_{in} n) + o[n] \\ &\simeq x[n] + e_g[n] + e_\tau[n] + o[n] \end{aligned} \tag{3}$$

where e_g and e_τ are error signals arising from the the gain and time errors respectively and the approximation in (3) arises by noting that $g[n]\tau[n] \simeq 0$.

If the input is a sinusoid, as per (2), we have:

$$e_g[n] = \mathcal{A} g[n] sin(\omega_{in} n + \phi), \quad \text{and,} \tag{4}$$

$$e_\tau[n] = \mathcal{A}\tau[n]\omega_{in} sin\left(\omega_{in} n + \phi + \frac{\pi}{2}\right) \tag{5}$$

as $e_g[n]$ and $e_\tau[n]$ have components at the same frequencies but with a 90° phase shift making them orthogonal we can

[1] Small angle approximation: $\cos(\tau[n]) \simeq 1$, and $\sin(\tau[n]) \simeq \tau[n]$.

do a joint estimation and modelling approach, accordingly we rewrite (4) and (5) as:

$$e_\zeta[n] \triangleq e_g[n] + e_\tau[n] = \mathcal{A}\mathbb{R}\mathrm{e}\left(e^{-j\phi}\zeta[n]e^{-j\omega_{in}n}\right) \quad (6)$$

where $\zeta[n] \triangleq \zeta_{n(\mathrm{mod}\,M)}$ and $\zeta_m = \tau_m\omega_{in} + jg_m$. From here onward we shall attempt to measure $\tilde{\zeta}_m \simeq \zeta_m$ first and then use these to compute estimates of g_m and τ_m:

$$\tilde{g}_m = \mathbb{I}\mathrm{m}(\tilde{\zeta}_m) \quad \text{and} \quad \tilde{\tau}_m = \frac{1}{\omega_{in}}\mathbb{R}\mathrm{e}(\tilde{\zeta}_m) \quad (7)$$

We now consider the spectrum of these terms in turn:

1) Spectrum of $o[n]$: As $o[n] \triangleq o_{n(\mathrm{mod}\,M)}$ is a periodic function having period M, it is fully defined by the length M sequence $\{o_m\}$ or equivalently its M-point DFT, $\{O_a\}$. Accordingly, we have the iDFT relation:

$$o[n] = \frac{1}{M}\sum_{a=0}^{M-1} O_a e^{ja\frac{2\pi}{M}n} \quad \forall\ n \quad (8)$$

From (8) it is clear that O_a is the complex amplitude[2] of the tones having normalized frequency $a\frac{2\pi}{M}$ rads/sample for all $0 \le a < M$ present in $o[n]$, a fact that will be exploited in Section III-A below.

2) Spectrum of $\zeta[n]$: By the same logic as above we have:

$$\zeta[n] = \frac{1}{M}\sum_{a=0}^{M-1} Z_a e^{ja\frac{2\pi}{M}n} \quad \forall\ n$$

where the $\{Z_a\}$ is defined as the M-point DFT of $\{\zeta_m\}$.

Substitute into (6) yields:

$$\begin{aligned} e_\zeta[n] &= \frac{\mathcal{A}}{2}\left(a^{-j\phi}\zeta[n]e^{-j\omega_{in}n} + e^{j\phi}\zeta^*[n]e^{j\omega_{in}n}\right) \\ &= \frac{\mathcal{A}}{2M}\left(e^{-j\phi}\sum_{a=0}^{M-1} Z_a e^{j(a\frac{2\pi}{M}-\omega_{in})n}\right. \\ &\quad \left. + e^{j\phi}\sum_{a=0}^{M-1} Z_a^* e^{j(a\frac{2\pi}{M}+\omega_{in})n}\right) \end{aligned} \quad (9)$$

Accordingly, we note that the amplitudes of the tones having normalized frequencies $a\frac{2\pi}{M} \pm \omega_{in}$ rads/samples present in $e_\zeta[n]$ are given by $\frac{\mathcal{A}}{2}e^{j\phi}Z_a^*$ and it's conjugate respectively.

B. TIADC With Nonlinear Front End and Sinusoidal Input

ADCs always have an AFE that may introduce the nonlinear tones, the most prominent SFDR-limiting spur is the third-order harmonic (HD3). We propose a novel nonlinear model to replace the more conventional complete Volterra series based system, which is supported by the experimental data in Section VI. The output of TIADC with the nonlinear response (HD3) and time-interleaved mismatch from (3) can be written as:

$$y[n] \simeq \alpha_1 x[n] + \alpha_3 x^3[n-D] + e_g[n] + e_\tau[n] + o[n] \quad (10)$$

where α_k as the amplitude of the k^{th} harmonic ($k = 1$ corresponds to the fundamental) and D is the fractional delay of the HD3 component (assumed constant, independent of inputs signal frequency).

[2]The O_a are independent of the amplitude and frequency of the input signal.

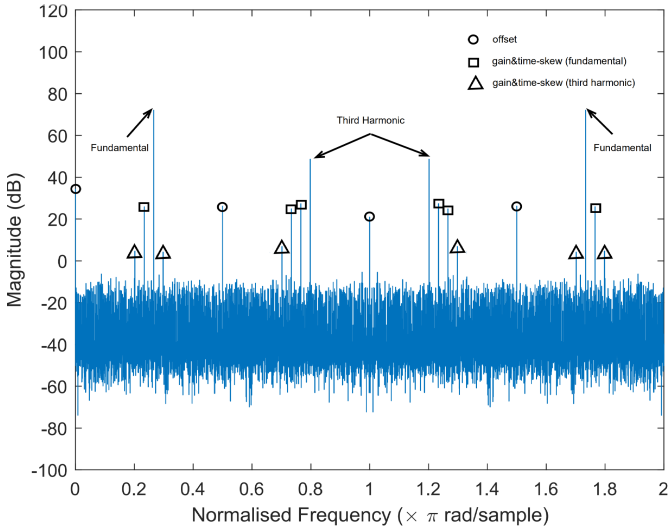

Fig. 1. The PSD for the 4-channel TIADC model suffering from nonlinearity spurs and offset, gain, and time-skew mismatch from 0 to 2π for the normalized angular frequency. ○ represents the offset spurs, □ shows the gain and time-skew mismatches caused by the fundamental signal, and △ is the gain and time-skew mismatches caused by the third harmonic.

An example of the frequency spectrum of 4-channel TIADC with a nonlinear front-end and suffering from the offset, gain, and time-skew mismatches are depicted in Fig. 1. The gain and time-skew mismatch tones caused by the third harmonic are minor to be neglected, but we still label them in the figure. As previously noted, the $e_t[n]$ and $e_g[n]$ components are located at the same position in the frequency domain and so are jointly labelled.

III. Mismatch Calibration

This algorithm considers the amplitude and phase of fundamental and the spurs caused by offset, gain, and time-skew mismatches. As we know the frequency of fundamental, the positions of the spurs caused by fundamental signal have fixed locations from 0 to F_s in the frequency domain. The amplitude and phase of these spurs can be measured using the multi-tone ground truth estimation [34]. The result can be returned by the complex value, and the mismatches can be estimated from the information using the inverse of FFT. We consider the various mismatches in turn:

A. Offset Estimation

From (8) we know that the offset component $o[n]$ consists of the sum of M tones having complex amplitudes O_a and normalized frequencies $a\frac{F_s}{M}$ samples/sec. Assuming these frequencies do not overlap with anything other tones we can measure these as $\tilde{O}_a$ using standard frequency domain measurement techniques,[3] e.g. [34]. We know that the $\{O_a\}$

[3]We note of course that, as $o[n]$ (and $y[n]$) is real-valued thus $\{O_a\}$ has conjugate symmetry which can be exploited during the estimation process.

are the M-point DFT of the $\{o_m\}$ and thus we have, in vector notation, the result:

$$\tilde{\boldsymbol{o}} = \text{iDFT}(\tilde{\boldsymbol{O}}).$$

One problem with this method is that it requires the use of the DC output from the ADC, i.e., O_0. This can be an unreliable measurement impacted by, for example, the physical coupling of the ADC, so its use should be avoided. In the vast majority of high-speed applications, any DC component present in the ADC's output is not important[4] and so it is not necessary to estimate (and remove) the O_0 term. Thus we typically implement the following algorithm instead:

$$\tilde{\boldsymbol{o}} = \text{iDFT}\left([0, \tilde{O}_1, \tilde{O}_2, \ldots, \tilde{O}_{M-1}]^T\right), \tag{11}$$

where we have simply replaced O_0 with zero which is proved in Appendix A.

The vector of correction values $\tilde{\boldsymbol{o}}$ obtained are correct up to an additive (unknown) error, and thus an arbitrary constant can be added to the correction values, $\tilde{\boldsymbol{o}}$, if desired which can bring some advantages. Section III-C discusses some possible options.

B. Gain & Time-Skew Estimation

Based on the discussion in II-A.2 and Provided the tones do not overlap in the frequency domain we can use standard standard frequency domain techniques, e.g. [34], to measure the complex amplitudes $\{E_a^+\}$ and $\{E_a^-\}$ of the tones having normalized frequency $a\frac{2\pi}{M} \pm \omega_{in}$ respectively. From these we then compute estimates of $\{\text{Z}_a\}$ as follows:

$$\begin{aligned} &\text{Z}_a \simeq \tilde{\text{Z}}_a \triangleq \frac{1}{2}\left(\tilde{\text{Z}}_a^- + (\tilde{\text{Z}}_a^+)^*\right) \quad \text{where,} \\ &\tilde{\text{Z}}_a^+ \triangleq \frac{2}{\mathcal{A}e^{j\phi}} E_a^+ \quad \text{and} \quad \tilde{\text{Z}}_a^- \triangleq \frac{2}{\mathcal{A}e^{-j\phi}} E_a^- \end{aligned} \tag{12}$$

Unfortunately, for $a = 0$ the tones do overlap with the fundamental frequency (the input signal). However, as argued in Appendix A, the sum of g_m and τ_m (and hence the zeroth DFT value) can be taken to be zero, and thus we let $\tilde{\text{Z}}_0 = 0$ always, and estimate all the other $\tilde{\text{Z}}_a$ for $1 \le a < M$ as described above thus avoiding the overlapping tone problem when $a = 0$.

One issue is that $\mathcal{A}$ and ϕ in (12) are unknowns and must be estimated from the measurement of the fundamental tone, i.e $E_0^+ \simeq \frac{1}{2}\mathcal{A}e^{j\phi}$, leading to the algorithm 1.

C. Estimate Modification Using Various Reference Options

As mentioned in Sub-Section III-A, we can add an arbitrary amount to the output of (11) affording us a degree of freedom to modify the vector of corrections, $\tilde{\boldsymbol{o}}$, as desired by the implementation:

$$\tilde{\boldsymbol{o}} \mapsto \quad \tilde{\boldsymbol{o}} - \lambda_{\text{offset}},$$

Common options for λ_{offset} are:

[4]So long as the DC component is sufficiently small so as not to significantly impact the ADC's dynamic range.

Algorithm 1 Frequency Domain Method for Estimating Gain and Timing Errors

Result: Gain, $\{\tilde{g}_m\}$, and timing, $\{\tilde{\tau}_m\}$, error estimates

1 Measure the complex amplitudes $\{E_a^+\}$ and $\{E_a^-\}$ of the tones having normalized frequency $a\frac{2\pi}{M} \pm \omega_{in}$ respectively.

2 Compute:

$$\tilde{\text{Z}}_a \simeq \begin{cases} 0 & a = 0 \\ \frac{1}{2}\frac{E_a^- + (E_a^+)^*}{(E_0^+)^*} & 1 \le a < M \end{cases}$$

3 Use iDFT to convert to time domain:

$$\tilde{\boldsymbol{\xi}} = \text{iDFT}\left(\tilde{\mathbf{Z}}\right)$$

4 Use (7) to compute $\{\tilde{g}_m\}$ and $\{\tilde{\tau}_m\}$.

- No modification:

$$\lambda_{\text{offset}} = 0$$

  in this case, the mean correction will be zero.
- Use the i^{th} sub-ADC as reference:

$$\lambda_{\text{offset}} = o_i$$

  in this case, no offset correction is applied to the i^{th} sub-ADC and all the others are essentially aligned to it.
- Mid-range reference [5]: Minimise the maximum absolute value of the offset correction.

$$\lambda_{\text{offset}} = \tfrac{1}{2}\left(\max_m\{\tilde{o}_m\} + \min_m\{\tilde{o}_m\}\right) \tag{13}$$

The mid-range approach, (13), is the best in the sense that it minimizes the dynamic range of the correction circuits (be they analog or digital).

The addition of an arbitrary time-skew constant to each sub-ADC's output serves only to impact the overall latency of the system which is typically not of concern affording us a degree of freedom to modify the time-skew estimates $\tilde{\boldsymbol{\tau}}$ as desired to facilitate implementation:

$$\tilde{\boldsymbol{\tau}} \mapsto \quad \tilde{\boldsymbol{\tau}} - \lambda_\tau,$$

typical options for λ_τ are:

$$\begin{aligned} &\lambda_\tau = 0, \quad \text{or,} \\ &\lambda_\tau = \tau_i, \quad i^{\text{th}} \text{ sub-ADC reference,} \quad \text{or,} \\ &\lambda_\tau = \frac{1}{2}\left(\max_m\{\tilde{\tau}_m\} + \min_m\{\tilde{\tau}_m\}\right) \end{aligned} \tag{14}$$

for, the zero mean, the i^{th} sub-ADC as a reference, or the mid-range correction solutions respectively.

The modification of the gain estimates, $\tilde{\boldsymbol{g}}$, from algorithm 1 is slightly more complex due to the multiplicative nature of the gain error correction. The degree of freedom that can be exploited here is each gain corrector can be adjusted by the same constant affecting only an overall gain shift which can generally be ignored in most applications. Thus the ratio of

$1+\tilde{g}_i$ to $1+\tilde{g}_j$ for all i, j must remain unchanged before and after the modification implying the following structure:

$$\tilde{\boldsymbol{g}} \mapsto \quad \lambda_{\text{gain}}\,(1+\tilde{\boldsymbol{g}}) - 1,$$

Common options for λ_{gain} are:

- No modification:

$$\lambda_{\text{gain}} = 1$$

  in this case the mean of the $\tilde{\boldsymbol{g}}$ is zero but this is not to say that the mean of the corrections, $\frac{1}{1+\tilde{g}_m}$, would be unity.
- Use the i^{th} sub-ADC as reference:

$$\lambda_{\text{gain}} = \frac{1}{1+\tilde{g}_i}$$

  In this case, no gain correction is applied to the i^{th} sub-ADC, and all the others are essentially aligned to it.
- Additive mid-range:

$$\lambda_{\text{gain}} = \frac{2}{(\max_m\{\tilde{g}_m\} + \min_m\{\tilde{g}_m\})} \tag{15}$$

  in this case, it is similar to the mid-range approach for offset and time-skew errors.
- Multiplicative mid-range: arrange maximum gain to be the same proportion above unity as the minimum gain is below, i.e. $\max_m\{\frac{1}{1+\tilde{g}_m}\} = 1/\min_m\{\frac{1}{1+\tilde{g}_m}\}$, accordingly:

$$\lambda_{\text{gain}} = \frac{1}{\sqrt{(1+\max_m\{\tilde{g}_m\})(1+\min_m\{\tilde{g}_m\})}} \tag{16}$$

Regarding offset and gain correction, the mid-range options for estimate modification, (13) and (16) are generally favoured by the authors of this paper; however, they have no bearing on the results as we assume no dynamic range limitations in the offset and gain digital correction circuits, so the various options are just presented here for completeness.

In Section V below that the mid-range method, (14), leads to a large reduction in the dynamic range resulting in better accuracy and higher production yields.

D. Pathological Cases

The foreground estimation is valid for a wide range of input frequencies of the sinusoidal wave as a testing signal; however, some frequencies are pathological cases in which we cannot separate the mismatch and harmonic tones. For example, when the input signal at any of the frequencies, $\frac{a}{2M}Fs,\ \forall a = \{1, 2, \ldots M\}$, where the spurs of the mismatch and harmonics overlap with themselves, hence, we cannot measure the amplitude and phase of each tone separately.

Fig. 2 depicts the examples of the pathological case for 4-channel TIADC. In Fig. 2(a), the input frequency of testing signal is $\frac{Fs}{4}$, the tones located at 0 and $\frac{Fs}{2}$ caused by offset, gain, and time-skew mismatch. The tones situate at $\frac{Fs}{4}$ and $\frac{3Fs}{4}$ consist of fundamental, harmonics, and mismatches. As shown in Fig. 2(b), the input frequency is $\frac{3F_s}{8}$, the offset spurs caused by fundamental coincide with the third harmonic. Thus, we cannot measure the amplitude and phase of mismatch tones alone.

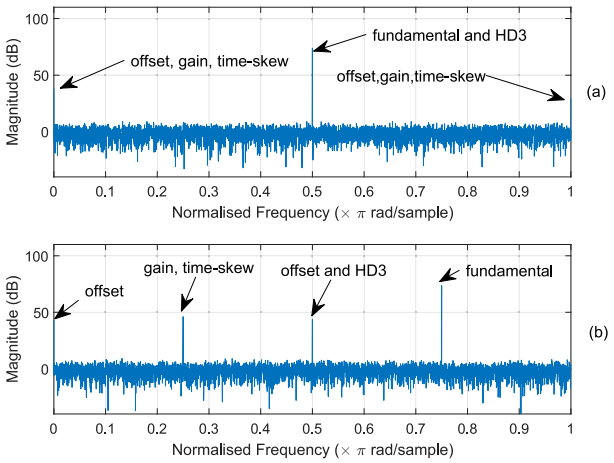

Fig. 2. Illustration of two pathological cases for a 4-channel TIADC (a) PSD showing nonlinearity, offset, gain and time-skew mismatch with the normalized input frequency is $\frac{Fs}{4}$, and (b) when the input frequency is $\frac{3Fs}{8}$. In both cases, it is not possible to uniquely identify the various components.

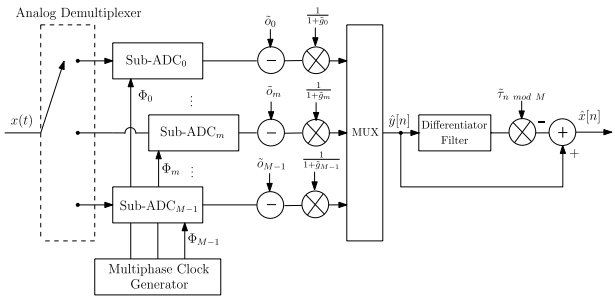

Fig. 3. Mismatch correction using the 1^{st} Taylor-based correction.

E. Mismatches Correction

Equipped with the offset and gain mismatches estimates, $\tilde{o}_m$ and $\tilde{g}_m$ respectively, we can corrected for these as follows:

$$\hat{y}[n] = \frac{y[n] - \tilde{o}_{n \bmod M}}{1+\tilde{g}_{n \bmod M}} \tag{17}$$

To compensate for the time-skew mismatch, we use Taylor-based correction as follows:

$$\hat{x}[n] \triangleq \hat{y}[n] - \big((h * \hat{y})[n]\big)\,\tau_{n \bmod M} \tag{18}$$

where $*$ is the convolution operator, and $\{h\}$ are the coefficients of a first-order differentiator filter. The system structure is shown in Fig. 3. Often the coefficients of a 1^{st} order differentiator filter are taken to be:

$$h[k] = \begin{cases} 0, & k = 0 \\ \frac{(-1)^k}{k}, & \text{otherwise} \end{cases} \tag{19}$$

where K is odd and $|k| \le \frac{K-1}{2}$.

However, these coefficients are not correct when the input frequency is not in the first Nyquist zone. The authors in [20] propose a differentiator filter design with the help of the Hilbert transform filter, which can adopt the input signal within any Nyquist zone. The magnitude response of the oversampling differentiator filter is shown in Fig. 4. It can compute the derivative of the input at about 90%

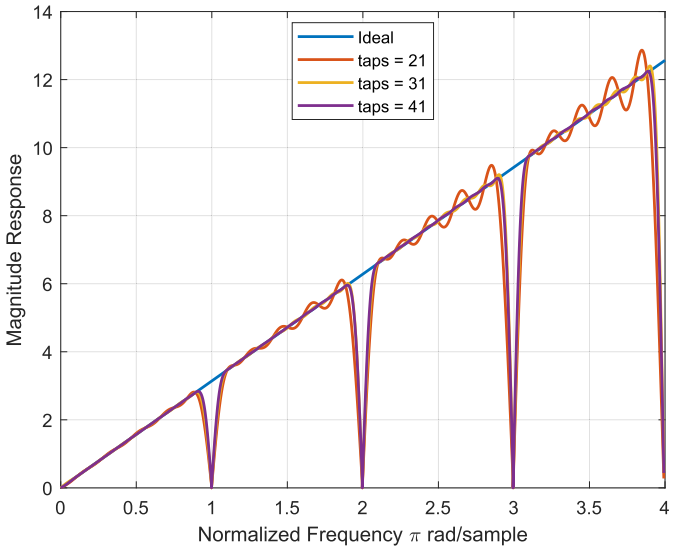

Fig. 4. The magnitude response of the oversampling differentiator filter design operating in any Nyquist zone.

(0.05–0.95) within any Nyquist zone making it suitable for many applications and is the filter used in our work.

IV. Nonlinearity Calibration

When the mismatch calibration is done we can consider the signal $\hat{x}[n]$ as being the sampled input signal plus the assumed non-linear terms (10) as follows:

$$\hat{x}[n] \simeq \alpha_1 x[n] + \alpha_3 x^3[n-D] \tag{20}$$

Provided $\alpha_3 \ll \alpha_1$ we can perform the following correction:

$$\begin{aligned}\tilde{x}[n] &= \hat{x}[n] - \left(\lambda \hat{x}[n-D]\right)^3 \\ &\approx \alpha_1 x[n] \quad \text{as required}\end{aligned} \tag{21}$$

where $\lambda \triangleq \frac{\sqrt[3]{\alpha_3}}{\alpha_1}$. The correction in (21) can introduce higher order terms, however, these terms can be neglected they should be smaller that the ADC noise floor. From our experimental work we found that the λ is not constant with respect to frequency, however D is, thus we propose to implement the correction in (21) using an FIR filter with a constant group delay (i.e. linear phase) and a magnitude response that is estimated through the repeated measurements of the fundamental's and HD3's amplitude and phase at many spot frequencies throughout the entire frequency band. Fig. 5 depicts the offline training process and the run-time process for the HD3 calibration / correction algorithms respectively.

In the training stage, we use K sinusoidal waves as test signals sweeping the frequency across the full band of operation. The amplitude and phase of the fundamental and HD3, $\{\tilde{\alpha}_1(\omega), \tilde{\phi}_1(\omega), \tilde{\alpha}_3(\omega), \tilde{\phi}_3(\omega)\}$, are measured using the multi-tone ground truth estimation algorithm for each sinusoidal input. Using this information we can estimate the amplitude response of our correction filter as follows:

$$\tilde{\lambda}(\omega) = \frac{\sqrt[3]{\tilde{\alpha}_3(\omega)}}{\tilde{\alpha}_1(\omega)} \tag{22}$$

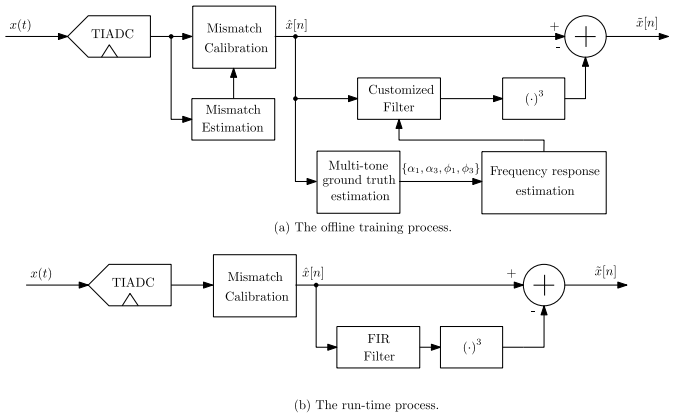

Fig. 5. (a) The offline training process for nonlinear correction. (b) The run-time process and the coefficients of the FIR filter are copied from the offline training.

and the group delay $\tilde{D}$ can be estimated by linearly regressing that quantity $\frac{1}{3}\tilde{\phi}_3(\omega) - \tilde{\phi}_1(\omega)$ with respect to frequency. Equipped with our estimate of $\tilde{D}$ and the magnitude response, $\tilde{\lambda}(\omega)$, we use standard filter design techniques to create the FIR filter coefficients.

V. Statistic Analysis for Reference Selection

In this section, we use the time-skew mismatch as an example to do statistic analysis for various reference options mentioned in Section III-C. An appropriate time reference improves the accuracy of the 1^{st} Taylor-based correction due to reducing the dynamic range of the correction. The amount of correction of each sub-ADC is defined as:

$$\dot{\tau}_m \triangleq \tau_m - \lambda_\tau$$

We use the statistic probability defined as η to evaluate the target yield for different references as follows:

$$\eta \triangleq \mathrm{P}\left(|\dot{\tau}_m| \le \Delta \quad \forall 0 \le m < M\right)$$

where Δ is defined as a dynamic correction range.

A. Dynamic Correction Range for Conventional Reference Selections

From (14), conventional time references are listed as following:

- Choosing $\lambda_\tau = 0$, or $\lambda_\tau = \frac{1}{M}\sum_{m=0}^{M-1}\tau_m$, which are same as we have derived the mean of time-skew mismatch is zero. To do the statistic analysis, the constraint on Δ can be written as:

$$\Delta = \sqrt{2}\sigma_\tau \mathrm{erf}^{-1}\left(\eta^{\frac{1}{M}}\right)$$

  where $\mathrm{erf}^{-1}(\cdot)$ is the inverse of error function.
- In [16] and [17], one of the main sub-ADC is used as the time reference. As an example, $\lambda_\tau = \tau_0$, and the constraint on Δ is following as:

$$\Delta = 2\sigma_\tau \mathrm{erf}^{-1}\left(\eta^{\frac{1}{M-1}}\right)$$

- In [18], an extra sub-ADC is used as the time reference, and the constraint can be written as:

$$\Delta = 2\sigma_\tau \text{erf}^{-1}\left(\eta^{\frac{1}{M}}\right)$$

B. Dynamic Correction Range for Mid-Range Reference Selection

The authors in [5] propose a mid-range solution as time reference can be written as follows:

$$\lambda_\tau = \frac{\text{Max}_m(\{\tau_m\}) + \text{Min}_m(\{\tau_m\})}{2}$$

As this λ_τ does not follow normal distribution; thus, we use $\text{Max}(\dot{\tau}_m)$ to evaluate the Δ, and it can be defined as:

$$\text{Max}(\dot{\tau}_m) \triangleq \frac{\text{Max}_m(\{\tau_m\}) - \text{Min}_m(\{\tau_m\})}{2} \tag{23}$$

The probability distribution of $\text{Max}(\tau_m)$ is an extreme order distribution, and the PDF of $\text{Max}(\tau_m)$ can be well approximated by gamma distributions with appropriate parameters in [36], and it can be written as:

$$\text{P}\left(\text{Max}(\tau_m)\right) = M\Phi(\text{Max}(\tau_m))^{(M-1)}\phi(\text{Max}(\tau_m)) \tag{24}$$

where $\Phi(\cdot)$ is the cumulative distribution function (CDF) and $\phi(\cdot)$ is the probability distribution function of standard Gaussian distribution.

The (24) can be approximated by the gamma distribution with parameters, $(\text{Max}(\tau_m) - c) \sim \Gamma(k, \theta)$. The location parameter defined as c can be expressed as:

$$c \triangleq \left(2.8989\ln(\log_2(M)) - 4.4291\right)\sigma_\tau$$

The shape parameter defined as k can be written as:

$$k \triangleq \frac{\left(E_M - \frac{c}{\sigma_\tau}\right)^2}{S_M^2}$$

The scale parameter defined as θ can be denoted as:

$$\theta \triangleq \frac{S_M^2}{E_M - \frac{c}{\sigma_\tau}}\sigma_\tau$$

where

$$S_M = 0.5\left(\Phi^{-1}\left(0.8832^{\frac{1}{M}}\right) - \Phi^{-1}\left(0.2142^{\frac{1}{M}}\right)\right)$$
$$E_M = \Phi^{-1}\left(0.5264^{\frac{1}{M}}\right)$$

Fig 6 shows the PDF of the $\text{Max}(\tau_m)$ using math model and gamma distribution approximation with different sample sizes to verify the model. When M is small, the two distributions are the exactly same. In (23), we can assume $\text{Max}_m(\tau_m)$ and $\text{Min}_m(\tau_m)$ are independent. The PDF of $\text{Max}(\dot{\tau}_m)$ has a double shape parameter and a half scale parameter than the PDF of $\text{Max}_m(\tau_m)$, which is

$$(\text{Max}(\dot{\tau}_m) - c) \sim \Gamma\left(2k, \frac{\theta}{2}\right)$$

The Δ for mid-range reference can be denoted as:

$$\Delta \geq \frac{\theta}{2}\gamma^{-1}(\eta, 2k) + c$$

where $\gamma^{-1}(\cdot)$ is the inverse lower incomplete gamma function.

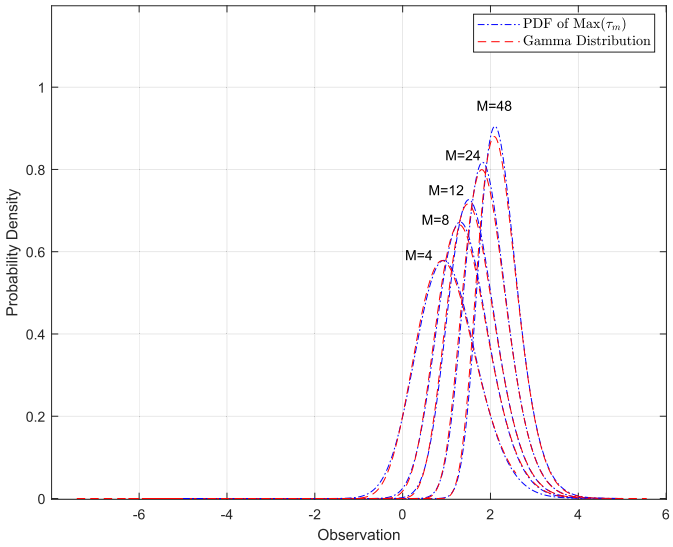

Fig. 6. Probability density functions of the max distributions of Gaussian sample with different sample sizes (M). The blue line is the numerical method and the red one is the gamma distribution approximation.

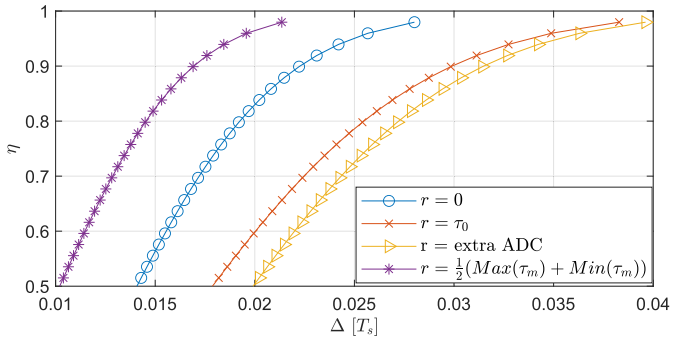

Fig. 7. The estimated CDF versus dynamic correction range using various time reference options.

C. Statistic Analysis

Fig. 7 depicts when the RMS of τ_m is $0.01T_s$, using the mid-range as time reference reaches more than 95% probability to make the corrected region less than 0.02, and using the zero, anyone sub-ADC, or extra ADC as time reference can only reach 80%, 60% and 50% respectively. Thus, the mid-range is the best time-skew reference to reduce the dynamic correction range.

VI. Results

This work is carried out using the Xilinx Zynq UltraScale+ RFSoC ZCU111 evaluation kit. This platform contains a 12-bit, 4.096 GHz TI-ADC with 8 sub-ADCs. The raw data from the tool is in TDMS format, which must be converted to a suitable format that can be operated in Matlab. The laboratory experimentation setup is done on the PYNQ open-source platform to capture the raw data. This section comprises three parts. Firstly the experimental laboratory setup for capturing raw data from a ZCU111 board is briefly described. This is followed by the offline digital calibration demonstration (uses the real data captured from the experimental setup). Finally,

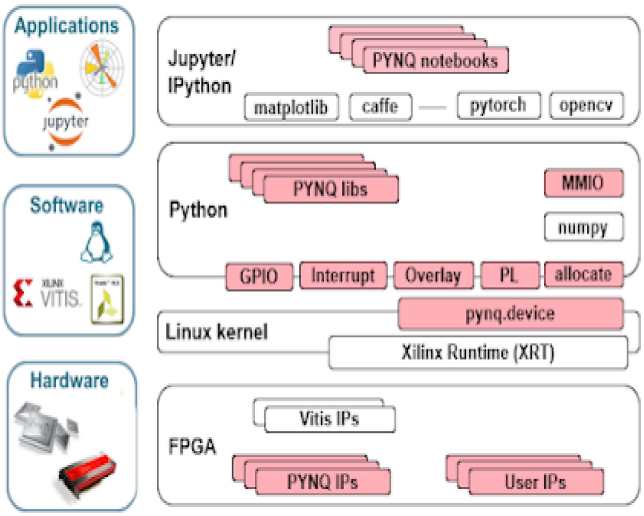

Fig. 8. An overview of the PYNQ platform (source: www.pynq.io).

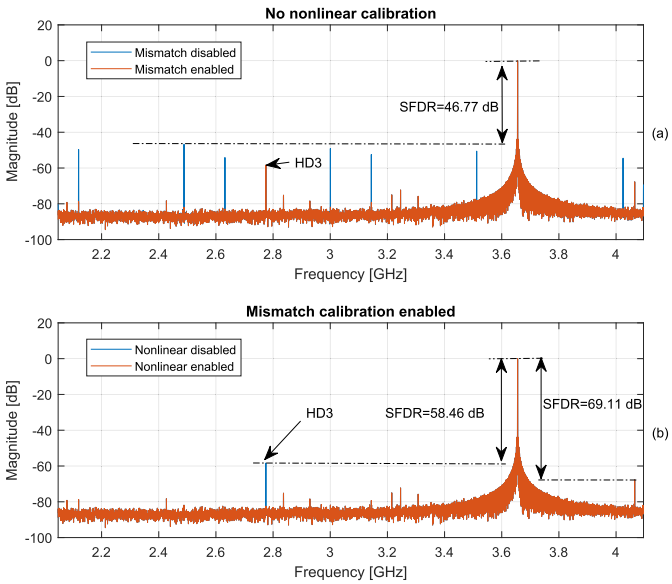

Fig. 9. Output spectra from an 8-channel TIADC with aggregate sampling rate 4.096 GHz, and a -1 dBFs sinusoidal input signal with frequency ≃3.66 GHz. (a) with no non-linear calibration: mismatch calibration enabled (red) / disabled (blue) and (b) with mismatch calibration enabled: nonlinear calibration enabled (red) / disabled (blue).

in Section VI-C we present a Monte Carlo simulation to verify the impact of time reference selection on the 1^{st} order Taylor-based correction.

A. Data Acquisition

PYNQ is an open-source project from Xilinx that makes it easier to use Xilinx platforms, which allows Python to run on a Linux kernel on the Processing System (PS) section of the RFSoC. The PYNQ platform presents itself as a server which can be accessed on a local area network. The developers can use hardware libraries and overlays on the programmable logic, which can speed up software running on a Zynq, and customize the hardware platform and interfaces. Fig. 8 depicts the overview of the PYNQ platform. We implemented some programmable logic to capture the real-time data from an ADC sampling at a rate of 4.096 GHz (8 parallel samples each at a rate of 512 MHz) and transfer these to on board DDR RAM for future offline processing. Each capturing process produced a block of 64k samples.

B. Digital Calibration Experimental Results

Firstly we need to compute the offset, gain and timing errors using the algorithm described in Section III which in principle should be the same for all frequency points - however in practice we actually perform this 100 times using different input sinusoidal frequencies (sweep across the full band of operation) and compute a flat average.

Now with this set of mismatch parameters frozen we estimate the amplitude and phase for fundamental and HD3 and design the customized filter according to the algorithm in Section IV. This is done using the same set of previously captured data samples. Fig. 9 depicts the measured power spectral density (PSD) of the original raw data and illustrates the impact of enabling mismatch and / or nonlinear calibration. The input signal is a 3.66 GHz, -1 dBFs sinusoidal signal located at the second Nyquist zone. (a) shows the measured PSD of TIADC with mismatch calibration alone. The SFDR increase from 46.77 dB to 58.46 dB when we enable the mismatch calibration. Fig. 9(b) depicts the harmonic distortion correction result when the mismatch calibration is enabled. It is clear that the HD3 is removed and the SFDR performance significantly improves to 69.11 dB.

Fig. 10 depicts the performance result of the SFDR versus the input frequencies at the second Nyquist zone. The SFDR has around 14 dB improvement for the mismatch calibration alone and has another improvement ranging from 4 to 12 dB when the nonlinear correction is enabled. The amplitude of HD3 is larger when the input frequencies increase that why the mismatch enabled and nonlinear disabled curve (red) drops quickly at the high frequencies.

A brief comparison indicating the hardware complexity of the proposed FFT-based mismatch calibration algorithm and the prior FFT-based methods in [14], [21], and [22] are presented in Table I. We assume the length of sample data for the calibration is N. Note that, for all these FFT-based techniques, the estimation accuracy increases with the number of N; however, a larger N will lead to greater computational complexity.

C. Monte Carlo Simulation for Time-Skew Reference

In Section V, we state that the selection of time reference affects the time-skew correction range and further influences the performance of the Taylor-based correction. We verified it using the Monte Carlo simulation for $10,000$ time-skew sets (10,000 TIADC instances) with the RMS, $\sigma_\tau = 0.01T_s$. Fig. 11 depicts the histogram and cumulative distribution function (CDF) curve of the SNDR for 10-bit, 8-channel TIADC with three various reference options. The average SNDR for these cases is 60.12, 60.66 and 60.79 dB respectively. Fig. 12 does the same simulation but with 12-bit TIADC. It is clear

TABLE I

COMPARISON MISMATCH CALIBRATION OF OUR WORK WITH OTHER PRIOR FFT-BASED TECHNIQUES

Characteristics	[21]	[14]	[22]	This work
Calibration routine	Foreground	Background	Foreground	Foreground
Number of sub-ADC	M	2	M	M
Mismatch source	offset, gain	offset, gain, time-skew	gain, time-skew	offset, gain, time-skew
Time-skew reference	not mentioned	one specific sub-ADC	one specific sub-ADC	mid-range
Estimation multiplications	$\frac{N}{2}\log_2 N$	$\frac{N}{2}\log_2 N + \frac{N}{2}\log_2 \frac{N}{2}$	$\frac{N}{2}\log_2 \frac{N}{M}$	$\frac{N}{2}\log_2 N$
Estimation additions	$N\log_2 N$	$N\log_2 N + N\log_2 \frac{N}{2}$	$N\log_2 \frac{N}{M}$	$N\log_2 N$
Correction Complexity	offline training M additions for offset M multiplication for gain	L-tap adjustable fractional-delay filter needs $(L+1)^2 + L$ multiplications $4(L+1)$additions	offline training M multiplications for gain $M-1$ K-tap differentiator filters	offline training M additions for offset M multiplication for gain a K-tap differentiator filter

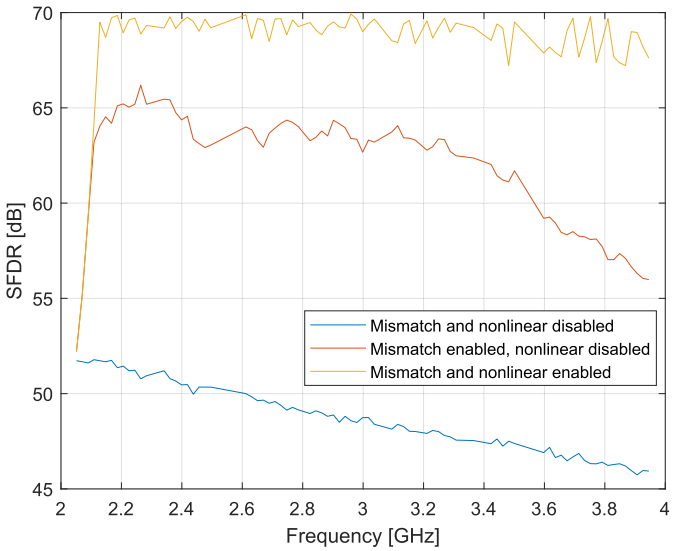

Fig. 10. The measured SFDR versus input frequencies at the second Nyquist zone. The blue line is both mismatch and nonlinear calibrations disabled. The red line is the mismatch calibration enabled and nonlinear calibration disabled. The yellow line is both mismatch and nonlinear calibrations enabled.

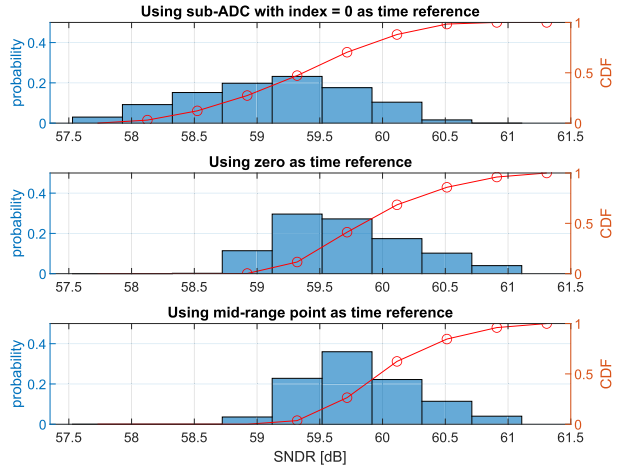

Fig. 11. Histogram (blue) and cumulative distribution function (CDF) curve (red) for SNDR for a 10-bit TIADC in Monte Carlo simulation. (a) Using one sub-ADC as λ_τ. (b) Using $\lambda_\tau = 0$ as time reference. (c) Using mid-range as λ_τ.

that choosing the mid-range as the time reference has a much better performance than using one sub-ADC as the

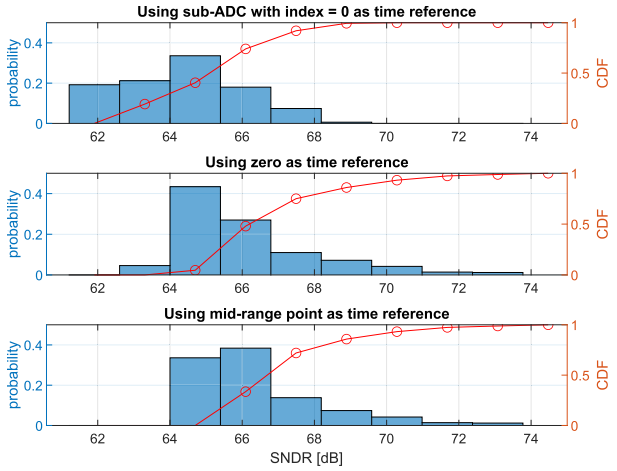

Fig. 12. Same as Fig. 11 but with a 12-bit TIADC.

time reference for the Taylor-based time-skew correction. Most previous FFT-based estimation methods [14], [22], [23] must use one sub-ADC as the time reference, which may degrade the performance of the time-skew correction.

VII. CONCLUSION

In this paper, we considered a time-interleaved ADC (TIADC) with a non-linear front end containing memory. We proposed a novel simplified non-linear model in place of the more complex conventional Volterra series based structure. We demonstrated pathological cases whereby the presence of the non-linear front end can cause the time-interleaving mismatch estimation algorithms to misbehave. Accordingly, we presented foreground estimation algorithms for both the time-interleaved mismatches and the non-linear parameters that are mutually compatible.

For time-skew mismatch, we designed an oversampling differentiator filter enabling our algorithm to function in any Nyquist zone. We also presented statistical analysis, supported by Monte Carlo simulation, for the time reference selection. This work clearly showed significant benefits for using the 'mid-range' time-skew reference option compared to, e.g. selecting one specific sub-ADC. The non-linear correction part of our system is comparatively simple due to the nature of our assumed non-linear impairment - the whole correction

process (at run-time) is implemented with one FIR filter and a cubic operation.

Our proposed calibration techniques were all verified using the Xilinx Zynq UltraScale+ RFSoC ZCU111 evaluation kit in conjunction with the PYNQ software platform and Matlab. We captured the raw data in the frequency band from 2.048 GHz to 4.096 GHz in the second Nyquist zone. We tested our calibration algorithms in Matlab using the raw data captured from the ADC board. Accordingly, we demonstrate an SFDR improvement of 14 dB with the mismatch calibration alone, and another improvement ranging from 4 to 12 dB when the nonlinear correction was also enabled. These results verify the correctness of our assumed simplified non-linear model and the associated calibration algorithms.

APPENDIX A

To prove $\sum_m o_m = \sum_m g_m = \sum_m \tau_m = 0$, we use the offset mismatch as an example and show that there exists an offset reference r_o that makes $\sum_m o_m = 0$ for any set of offset error. Starting with the DFT of the offsets:

$$O_k = \sum_{n=0}^{M-1} o_n w^{nk} = \begin{cases} \sum_{n=0}^{M-1} o_n & k = 0 \\ \sum_{n=0}^{M-1} o_n w^{nk} & k = 1 \dots M-1, \end{cases}$$

where we define w^{nk} is the (n^{th}, k^{th}) entry in the DFT matrix.

Because $\sum_{n=0}^{M-1} w^{nk} = 0$ for $k = 1 \dots M-1$, we can obtain $\sum_{n=0}^{M-1}(o_n - r_o)w^{nk} = \sum_{n=0}^{M-1} o_n w^{nk}$ for $k = 1 \dots M-1$ and for any reference scalar r_o thus:

$$O_k = \sum_{n=0}^{M-1}(o_n - r_o)w^{nk} \quad \forall \quad k = 1 \dots M-1$$

The above is an under-defined set of equations. The length M vector of offset corrections to be corrected for $\tilde{\boldsymbol{o}} \triangleq \{o_n - r_o\}$ can be estimated from the length $M-1$ vector of O_k's (for $k = 1$ to $M-1$) using the Moore-Penrose pseudo inverse and will correspond to that set of values having the zero mean, which means $O_0 = 0$ and $\sum_m o_m = 0$. We can also prove $\sum_m g_m = \sum_m \tau_m = 0$ using the same method.

ACKNOWLEDGMENT

The authors would like to thank China Scholarship Council supports for this work.

REFERENCES

[1] N. Kurosawa, H. Kobayashi, K. Maruyama, H. Sugawara, and K. Kobayashi, "Explicit analysis of channel mismatch effects in time-interleaved ADC systems," *IEEE Trans. Circuits Syst. I, Fundam. Theory Appl.*, vol. 48, no. 3, pp. 261–271, Mar. 2001.

[2] C. Vogel, "The impact of combined channel mismatch effects in time-interleaved ADCs," *IEEE Trans. Instrum. Meas.*, vol. 54, no. 1, pp. 415–427, Feb. 2005.

[3] J. Elbornsson, F. Gustafsson, and J.-E. Eklund, "Analysis of mismatch effects in a randomly interleaved A/D converter system," *IEEE Trans. Circuits Syst. I, Reg. Papers*, vol. 52, no. 3, pp. 465–476, Mar. 2005.

[4] X. Wang, F. Li, W. Jia, and Z. Wang, "A 14-bit 500-MS/s time-interleaved ADC with autocorrelation-based time skew calibration," *IEEE Trans. Circuits Syst. II, Exp. Briefs*, vol. 66, no. 3, pp. 322–326, Mar. 2019.

[5] A. Salib, M. F. Flanagan, and B. Cardiff, "A generic foreground calibration algorithm for ADCs with nonlinear impairments," *IEEE Trans. Circuits Syst. I, Reg. Papers*, vol. 66, no. 5, pp. 1874–1885, May 2019.

[6] Y. Wang, H. Xu, H. Johansson, Z. Sun, and J. J. Wikner, "Digital estimation and compensation method for nonlinearity mismatches in time-interleaved analog-to-digital converters," *Digit. Signal Process.*, vol. 41, pp. 130–141, Jun. 2015.

[7] Y. A. Tavares and M. Lee, "A foreground calibration for M-channel time-interleaved analog-to-digital converters based on genetic algorithm," *IEEE Trans. Circuits Syst. I, Reg. Papers*, vol. 68, no. 4, pp. 1444–1457, Apr. 2021.

[8] M. Seo, M. J. W. Rodwell, and U. Madhow, "Comprehensive digital correction of mismatch errors for a 400-Msamples/s 80-dB SFDR time-interleaved analog-to-digital converter," *IEEE Trans. Microw. Theory Techn.*, vol. 53, no. 3, pp. 1072–1082, Mar. 2005.

[9] M. El-Chammas and B. Murmann, "A 12-GS/s 81-mW 5-bit time-interleaved flash ADC with background timing skew calibration," *IEEE J. Solid-State Circuits*, vol. 46, no. 4, pp. 838–847, Apr. 2011.

[10] Y. Qiu, J. Zhou, Y. Liu, X. He, N. Xie, and Y. Liu, "An adaptive blind calibration technique for frequency response mismatches in M-channel time-interleaved ADCs," *IEEE Trans. Circuits Syst. II, Exp. Briefs*, vol. 66, no. 4, pp. 702–706, Apr. 2019.

[11] Y. Qiu, Y.-J. Liu, J. Zhou, G. Zhang, D. Chen, and N. Du, "All-digital blind background calibration technique for any channel time-interleaved ADC," *IEEE Trans. Circuits Syst. I, Reg. Papers*, vol. 65, no. 8, pp. 2503–2514, Aug. 2018.

[12] J. Matsuno, T. Yamaji, M. Furuta, and T. Itakura, "All-digital background calibration technique for time-interleaved ADC using pseudo aliasing signal," *IEEE Trans. Circuits Syst. I, Reg. Papers*, vol. 60, no. 5, pp. 1113–1121, May 2013.

[13] S. M. Jamal, D. Fu, N. C.-J. Chang, P. J. Hurst, and S. H. Lewis, "A 10-b 120-Msample/s time-interleaved analog-to-digital converter with digital background calibration," *IEEE J. Solid-State Circuits*, vol. 37, no. 12, pp. 1618–1627, Dec. 2002.

[14] X. Bai, H. Hu, W. Li, and F. Liu, "Blind calibration method for two-channel time-interleaved analog-to-digital converters based on FFT," *J. Electron. Test.*, vol. 34, no. 6, pp. 643–650, Dec. 2018.

[15] A. Salib, M. F. Flanagan, and B. Cardiff, "A high-precision time skew estimation and correction technique for time-interleaved ADCs," *IEEE Trans. Circuits Syst. I, Reg. Papers*, vol. 66, no. 10, pp. 3747–3760, Oct. 2019.

[16] S. Chen, L. Wang, H. Zhang, R. Murugesu, D. Dunwell, and A. C. Carusone, "All-digital calibration of timing mismatch error in time-interleaved analog-to-digital converters," *IEEE Trans. Very Large Scale Integr. (VLSI) Syst.*, vol. 25, no. 9, pp. 2552–2560, Sep. 2017.

[17] C.-Y. Lin, Y.-H. Wei, and T.-C. Lee, "A 10-bit 2.6-GS/s time-interleaved SAR ADC with a digital-mixing timing-skew calibration technique," *IEEE J. Solid-State Circuits*, vol. 53, no. 5, pp. 1508–1517, May 2018.

[18] E. Iroaga, B. Murmann, and L. Nathawad, "A background correction technique for timing errors in time-interleaved analog-to-digital converters," in *Proc. IEEE Int. Symp. Circuits Syst.*, vol. 6, May 2005, pp. 5557–5560.

[19] D. Zhou, C. Talarico, and J. Silva-Martinez, "A digital-circuit-based evolutionary-computation algorithm for time-interleaved ADC background calibration," in *Proc. 29th IEEE Int. Syst. Chip Conf. (SOCC)*, Sep. 2016, pp. 13–17.

[20] M. Guo, J. Mao, S. W. Sin, H. Wei, and R. P. Martins, "A 1.6-GS/s 12.2-mW seven-/eight-way split time-interleaved SAR ADC achieving 54.2-dB SNDR with digital background timing mismatch calibration," *IEEE J. Solid-State Circuits*, vol. 55, no. 3, pp. 693–705, Mar. 2020.

[21] J. M. D. Pereira, P. M. B. S. Girão, and A. M. C. Serra, "An FFT-based method to evaluate and compensate gain and offset errors of interleaved ADC systems," *IEEE Trans. Instrum. Meas.*, vol. 53, no. 2, pp. 423–430, Apr. 2004.

[22] L. Guo, S. Tian, and Z. Wang, "Estimation and correction of gain mismatch and timing error in time-interleaved ADCs based on DFT," *Metrology Meas. Syst.*, vol. 21, no. 3, pp. 535–544, Aug. 2014.

[23] Y. Kuojun, S. Jiali, and Y. Huizhi, "A TIADC mismatch calibration method for digital storage oscilloscope," in *Proc. 13th IEEE Int. Conf. Electron. Meas. Instrum. (ICEMI)*, Oct. 2017, pp. 379–383.

[24] H. Liu and H. Xu, "An adaptive blind frequency-response mismatches calibration method for four-channel TIADCs based on channel swapping," *IEEE Trans. Circuits Syst. II, Exp. Briefs*, vol. 64, no. 6, pp. 625–629, Jun. 2017.

[25] B. Murmann, "Digitally assisted analog circuits," *IEEE Micro*, vol. 26, no. 2, pp. 38–47, Mar. 2006.
[26] A. M. A. Ali et al., "A 12-b 18-GS/s RF sampling ADC with an integrated wideband track-and-hold amplifier and background calibration," *IEEE J. Solid-State Circuits*, vol. 55, no. 12, pp. 3210–3224, Dec. 2020.
[27] A. Panigada and I. Galton, "A 130 mW 100 MS/s pipelined ADC with 69 dB SNDR enabled by digital harmonic distortion correction," *IEEE J. Solid-State Circuits*, vol. 44, no. 12, pp. 3314–3328, Dec. 2009.
[28] L. Shi, W. Zhao, J. Wu, and C. Chen, "Digital background calibration techniques for pipelined ADC based on comparator dithering," *IEEE Trans. Circuits Syst. II, Exp. Briefs*, vol. 59, no. 4, pp. 239–243, Apr. 2012.
[29] F. van der Goes et al., "A 1.5 mW 68 dB SNDR 80 Ms/s 2 × interleaved pipelined SAR ADC in 28 nm CMOS," *IEEE J. Solid-State Circuits*, vol. 49, no. 12, pp. 2835–2845, Dec. 2014.
[30] J. K. Cavers, "Amplifier linearization using a digital predistorter with fast adaptation and low memory requirements," *IEEE Trans. Veh. Technol.*, vol. 39, no. 4, pp. 374–382, Nov. 1990.
[31] R. Raich and G. T. Zhou, "On the modeling of memory nonlinear effects of power amplifiers for communication applications," in *Proc. IEEE 10th Digit. Signal Process. Workshop, 2nd Signal Process. Educ. Workshop.*, Sep. 2002, pp. 7–10.
[32] D. D. C. Jabbour and P. Desgreys, *Digitally-Enhanced Mixed-Signal Systems*. London, U.K.: IET Press, 2019.
[33] T. Kihara, K. Miyakoshi, and T. Yoshimura, "Digital third-order nonlinearity correction for time-interleaved A/D converters with VCOs," in *Proc. IEEE Int. Symp. Circuits Syst. (ISCAS)*, May 2019, pp. 1–4.
[34] H. Shen and B. Cardiff, "Multi-tone ground truth estimation for ADC testing," in *Proc. 32nd Irish Signals Syst. Conf. (ISSC)*, Jun. 2021, pp. 1–5.
[35] H. L. Duc, D. M. Nguyen, C. Jabbour, P. Desgreys, O. Jamin, and V. T. Nguyen, "Fully digital feedforward background calibration of clock skews for sub-sampling TIADCs using the polyphase decomposition," *IEEE Trans. Circuits Syst. I, Reg. Papers*, vol. 64, no. 6, pp. 1515–1528, Jun. 2017.
[36] C.-C. Chen and C. W. Tyler, "Accurate approximation to the extreme order statistics of Gaussian samples," *Commun. Statist. Simul. Comput.*, vol. 28, no. 1, pp. 177–188, 1999.

Haoyang Shen (Graduate Student Member, IEEE) received the B.E. degree from the University College Dublin, Ireland, in 2019, where he is currently pursuing the Ph.D. degree with a focus on ADC digital calibration.

Adam Blaq (Graduate Student Member, IEEE) received the B.Sc. and M.E. degrees in electronic engineering from University College Dublin. He worked as a Digital Design/Verification Engineer at Xilinx. He was a recipient of the Intel Masters in Engineering Scholarship in 2021.

Deepu John (Senior Member, IEEE) received the B.Tech. degree in electronics and communication engineering from the University of Kerala, India, in 2002, and the M.Sc. and Ph.D. degrees in electrical engineering from the National University Singapore, Singapore, in 2008 and 2014, respectively. He is currently an Assistant Professor with the School of Electrical and Electronics Engineering, University College Dublin, Ireland. He was a Post-Doctoral Researcher with the Bio-Electronics Laboratory, National University Singapore, from 2014 to 2017. Previously, he worked as a Senior Engineer with Sanyo Semiconductors, Gifu, Japan. His research interests include low-power biomedical circuit design, energy-efficient signal processing, and edge computing. He served as a member of the Organizing Committee/Technical Program Committee for several IEEE conferences, including TENCON, ASICON, ISCAS, BioCAS, and ICTA. He was a recipient of the Institution of Engineers Singapore Prestigious Engineering Achievement Award in 2011, the Best Design Award at the Asian Solid State Circuit Conference in 2013, and the IEEE Young Professionals Region 10 Individual Award in 2013. He served as a Guest Editor for IEEE TRANSACTIONS ON CIRCUITS AND SYSTEMS—I: REGULAR PAPERS and IEEE OPEN JOURNAL OF CIRCUITS AND SYSTEMS. He currently serves as an Associate Editor for IEEE TRANSACTIONS ON BIOMEDICAL CIRCUITS AND SYSTEMS, IEEE TRANSACTIONS ON CIRCUITS AND SYSTEMS—II: EXPRESS BRIEFS, and Wiley *International Journal of Circuit Theory and Applications*.

Barry Cardiff (Senior Member, IEEE) received the B.Eng. degree from the Electronic Engineering Department, UCD, in 1992, the M.Eng.Sc. degree (by research), and the Ph.D. degree in digital signal processing (DSP) for wireless and optical communications, under the supervision of Prof. Tony Fagan with a thesis titled "Detection Techniques in Vector Systems in Communications" in 2011, as a Mature Student. He worked as a Design Engineer at Nokia Mobile Phone (U.K.) Ltd., from 1993 to 2001, working on some of world's more advanced and innovative products culminating in the role of Chief Engineer and as a Contributor to the 3GPP standardization process. He was moved to Ireland in 2001, to work as a Systems Architect at the Silicon and Software Systems (S3 Group), where he has working mainly on embedded hardware/software development projects with applications ranging from wireless communications to hearing aids. He has continued to work for S3 Group for several years after a break from 2007 to 2011. In September 2013, he joined as an Academic Staff at UCD to complement the teaching staff both in Dublin and in a joint collaboration in Beijing (BDIC). His research interests are in the area of DSP applications mainly in communication systems both in the theoretical analysis and practical advancement of such systems and power/complexity reduction techniques in circuit design, i.e. DSP algorithms for digitally assisted analog circuits.